A molecular dynamics study of an aqueous LiI solution between Lennard-Jones walls

E. Spohr and K. Heinzinger
Max-Planck-Institut für Chemie (Otto-Hahn-Institut), Mainz, Federal Republic of Germany

(Received 23 August 1985; accepted 6 November 1985)

An MD simulation of a 2.2 m aqueous LiI solution between 12-6 Lennard-Jones walls has been performed which extended over 19 ps at an average temperature of 283 K. The basic tetragonal cell contained 200 ST2 water molecules and eight ions of each kind described as Lennard-Jones spheres with an elementary charge at the center. The effect of the walls on the hydration shell of the ions is investigated by means of ion–water radial distribution functions. Anisotropic water pair correlation functions are reported in order to show specific structural features near the walls. Changes in translational and rotational motions of the water molecules near the walls are discussed by means of velocity and angular velocity autocorrelation functions and their spectral densities, respectively.

I. INTRODUCTION

The liquid structure in the neighborhood of a liquid/solid interface has been the concern of many investigations published during the last years. While statistical mechanical theories stuck mainly to the treatment of model atomic fluids near model walls (e.g., see Refs. 1 and 2) many experimentalists focused on the structural behavior of water and aqueous solutions near metal electrodes (e.g., see Refs. 3 and 4).

Since 1981 several computer simulation studies of liquid water between walls have been reported. Jönsson[5] studied the influence of rigid walls on water using the Monte Carlo method while Christou *et al.*,[6] Marchesi,[7] Barabino *et al.*,[8] Sonnenschein and Heinzinger,[9] and Lee *et al.*[10] performed MD studies using different water–water potentials and different types of continuous water–wall potentials of Lennard-Jones (LJ) form or of purely repulsive exponential form. Recently Townsend *et al.*[11] published results for a spherical cluster of 1000 ST2 water molecules confined by a repulsive exponential potential which are in agreement with previous simulations. Furthermore an MD simulation of CF water[12] near a rigid NaCl crystal has been performed by Anastasiou *et al.* All authors discussed the water structure by presenting oxygen and hydrogen atom density profiles, which showed in all cases more or less pronounced density oscillations near the walls, and orientational distribution functions of H_2O relative to the walls. So far no simulation of an electrolyte solution between walls has been reported.

In this paper we present the results of an MD study of a 2.2 m aqueous LiI solution between two (12-6)-LJ walls using the ST2 model for water–water interactions. We discuss the water structure in the interphase by means of anisotropic pair correlation functions and some changes in the hydration shell of the ions in Sec. III. Section IV gives the dynamical properties gained from velocity and angular velocity autocorrelation functions and the spectral densities of translational and rotational motion. The results are compared with the results of an MD simulation study of an isotropic 2.2 m LiI solution[13–15] and of a simulation for pure ST2 water between (12-6)-LJ walls.[9,16]

II. PAIR POTENTIALS AND DETAILS OF THE SIMULATION

In the present MD simulation of a 2.2 m LiI solution between two walls the basic periodic box contains 200 water molecules, eight cations, and eight anions. The side length L in the two directions (x, y) where periodic boundary conditions are employed is 18.68 Å. The system was adjusted with the walls fixed at $\pm$ 12.31 Å such that the density in the center of the lamina equals the experimental bulk density of 1.19 g/cm^3 and the pressure determined by the average forces acting on the walls is not too far from standard conditions.

The ST2 model[17] is employed for water–water interactions and the ions are modeled as (12-6) Lennard-Jones (LJ) spheres with an elementary charge in the center. For the water–water, ion–water, and the LJ part of the ion–ion potential the "shifted force potential" method is applied with a cutoff distance of 9.34 Å and the potential parameters are the same as in an MD simulation of an isotropic LiI solution.[13] In the calculation of the Coulombic part of the ion–ion interactions a method by Heyes[18] based on the Evjen method[19] for the evaluation of electrostatic potentials is adapted. Using the Evjen method for potential summation all ions in N_c image cells within a distance R_c from the basic box contribute directly to the potential at the location of an ion. If R_c is large compared to the side length L of the box the shell of cells becomes approximately circular. To include the effect of the cells outside the circle with radius R_c a multipole expansion of the ionic charge distribution is carried out for each cell separately keeping only the dipole moments. If the dipole moments which have the same magnitude for all cells are replaced by a constant dipole density and the shell is assumed to be circular the integration over the outer space can be performed yielding a correction potential that is added to the direct potential. In the present simulation $R_c = 9L$ and $N_c = 241$. The water–wall and ion–wall interactions are modeled by a 12-6 LJ potential acting only on the centers of mass of the particles with parameters ϵ and σ being those of the ST2-potential and the ion–water potentials, respectively.

After 9 ps of equilibration the simulation extended over

 0021-9606/86/042304-06$02.10

10 ps at an average temperature of 283 K without rescaling the kinetic energy.

III. STRUCTURAL RESULTS

A. Density profiles

Contrary to previous simulations of pure water[5–10] and of model liquids (see Ref. 20) the oxygen and hydrogen density profiles do not show any oscillatory behavior. Small inhomogeneities in density are mainly a consequence of the volume occupied by the ions, as minima in the water density profiles coincide with maxima in the ion density profiles. The ions are distributed in such a way that they are able to build at least a first hydration shell. As a 19 ps simulation seems to be not long enough to calculate the density profile of the ions with a sufficient degree of reliability no density profiles are shown here.

Lee *et al.*[10] showed that the magnitude of the density oscillations depends on the relative strength of the particle–wall and particle–particle interactions. Their simulation of ST2 water with removed charges and consequently weaker water–water interactions exhibited much higher density oscillations than the simulation of normal ST2 water. Hence, the absence of the density oscillations is completely in accordance with previous computer simulations as the average particle–particle interaction in the solution is even stronger here than in pure water and the total particle–wall interaction energy contributes less than 0.1% to the total energy of the system.

B. Ion–water radial distribution functions

Table I shows a set of characteristic values for the ion–water and water–water radial distribution functions (RDF). With the exception of the values r_{m1} and $g(r_{m1})$ in the LiH case, the determination of which is somewhat arbitrary due to the shallowness of the minimum as well as due to statistical error, the RDF's g_{LiO} and g_{LiH} do not exhibit significant changes when compared with those of the isotropic solution.[13] This is expected as the water–wall interactions are very weak compared to the strong hydration forces of the Li^+.

TABLE I. Characteristic values of the radial distribution functions $g_{xy}(r)$ for the 2.2 m LiI solution between Lennard-Jones type walls. R_i, r_{Mi}, and r_{mi} give the distances in Å where for the ith time g_{xy} is unity, has a maximum and a minimum, respectively.

xy	r_{M1}	$g(r_{M1})$	R_2	r_{m1}	$g(r_{m1})$	$n(r_{m1})$	$g(r_{M1})/g(r_{m1})$
LiO	2.12	16.8	2.36	2.92	0.00	6.1	
LiH	2.68	7.5	2.97	3.70	0.38	15.4	
IO	3.64	2.55	4.06	4.35	0.82	7.7	3.1
	(3.68	2.28	4.20	4.40	0.90	8.7	2.6)[a]
IH	2.71	1.81	3.01	3.4	0.46	6.4	3.9
	(2.70	1.62	3.02	3.4	0.57	6.7	2.9)[a]
OO	2.84	3.26	3.24	3.7	0.74	6.0	
OH	1.88	1.20	2.00	2.44	0.45	1.8	
HH	2.41	1.41	2.73	3.02	0.82	9.6	

[a] Data for the isotropic solution (Ref. 13).

In the case of the weakly hydrated iodide ion, however, a significant change in g_{IO} and g_{IH} can be detected. For comparison the values of the isotropic solution are given in Table I in parentheses. Figure 1 shows the RDF's from the present simulation (full lines) and those for the isotropic LiI solution (dashed lines) together with their corresponding running integration numbers.

Due to the steric effect of the walls the running integration numbers are always lower in the lamina yielding a hydration number of 7.7 (from the value of n_{IO} at the location of the first minimum) which has to be compared to 8.7 in the isotropic solution. Both RDF's exhibit a higher first maximum and a lower first minimum and the ratio $g(r_{M1})/g(r_{m1})$ is higher for both g_{IO} and g_{IH} in the present simulation. Additionally, if the distance at which g_{IO} equals 1 for the second time is taken as a measure of the radial localization of the hydration shell it is significantly narrower in this work than in the isotropic solution thus indicating an enhancement of hydration structure around the iodide anion.

A more detailed analysis of the shape of $g_{\mathrm{IO}}(r)$ as a function of the ion–wall distance which is not given here shows that the observed increase in structure is due to less competition with strongly hydrated Li^+ ions. The hydration shell of the iodide ions closest to the wall is less disturbed because they are surrounded by less cations than those in the center of the lamina.

C. Water structure

Some characteristic values for the total water–water RDF's are given in Table I. The RDF's are in the limits of statistical uncertainty the same as in the isotropic solution.

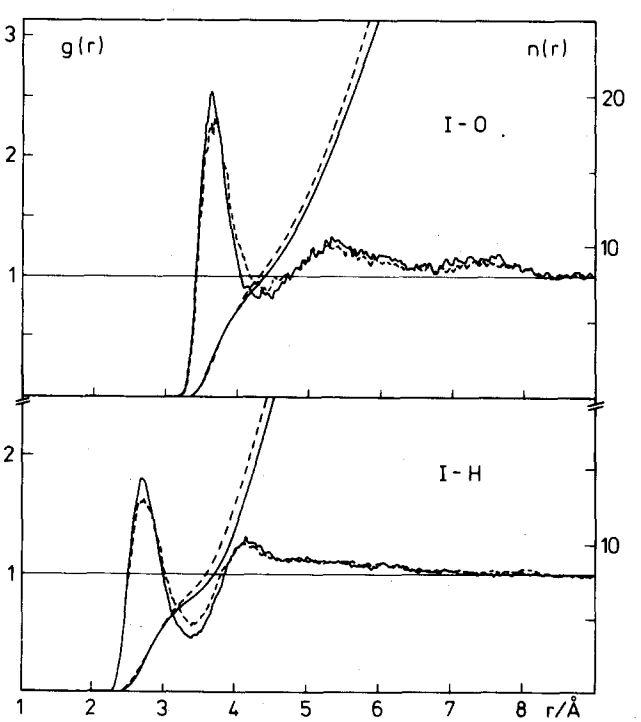

FIG. 1. Iodide–oxygen and iodide–hydrogen radial distribution functions $g(r)$ and running integration numbers $n(r)$ for the 2.2 m LiI solution confined between two Lennard-Jones walls (full lines) and for a bulk 2.2 m LiI solution (dashed lines).

Hence, for the investigation of the changes of the water structure induced by the walls the lamina is divided into 12 layers of 2 Å thickness and equivalent pairs are averaged. The RDF's g_{OO}, g_{OH}, and g_{HH} are calculated according to

$$g_{AB}(z_A, \cos\vartheta, r_{AB}) = \frac{\rho_{AB}^{(2)}(z_A, \cos\vartheta, r_{AB})}{\rho_A^{(1)}(z_A)\rho_B^{(1)}(z_A + r_{AB}\cos\vartheta)}, \quad (1)$$

where z_A is the z coordinate of particle A, r_{AB} the distance between A and B, ϑ the angle between r_{AB} and the wall normal $\hat{z}$ pointing into the solution, and $\rho^{(1)}$ and $\rho^{(2)}$ are the one and two particle densities as defined, e.g., by Vesely.[21]

The information contained in the three-dimensional histograms is evaluated in two different ways. Figure 2 shows all RDF's averaged over all directions of the interparticle vector. The full curves represent the RDF's for the two layers close to the wall ($|z| > 8.0$ Å), the dashed ones the corresponding functions for the inner part of the lamina. The inner layer radial distribution functions are identical with those calculated by Szasz *et al.*,[13] whereas the wall layer functions show a much more pronounced first hydration shell than pure bulk water[13,17] thus leading to the conclusion that the Lennard-Jones walls are very short-ranging structure makers. This is in accordance with the fact that the walls represent large unpolar species due to the choice of a one-dimensional water–wall potential. Regarding the fact that the water–wall interactions are much smaller than the residual interactions the increase in order of the first neighbor shell can be interpreted as the consequence of a smaller disturbance of a given pair of particles by the surrounding system.

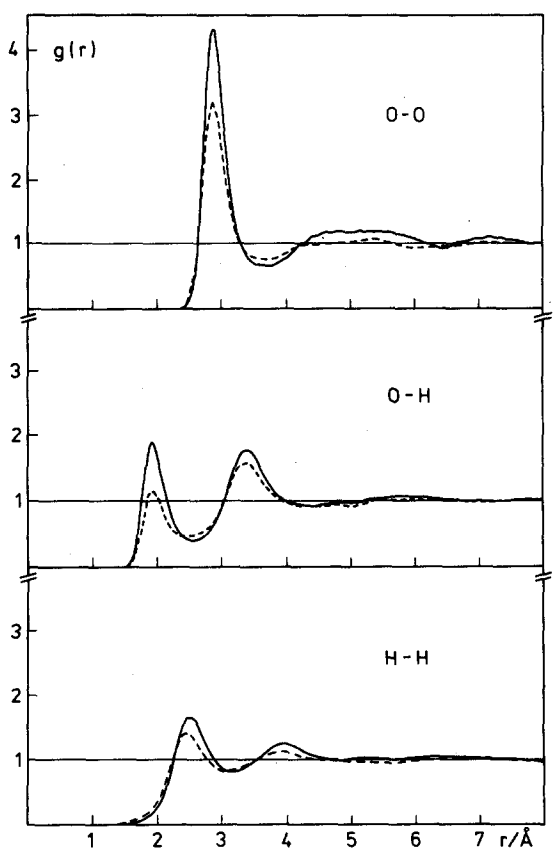

FIG. 2. Oxygen–oxygen, oxygen–hydrogen, and hydrogen–hydrogen radial distribution functions for the water molecules in a 2.2 m LiI solution between Lennard-Jones walls in the region close to the wall (full line) and in the interior of the lamina (dashed line).

This ordering effect is not found in the density profiles (see Sec. III A) because the second layer of water molecules is dominated by the effect of the ions. An analysis of the orientational distribution of the water dipole vectors relative to the walls (as carried out by Sonnenschein and Heinzinger[9]) is in accordance with this view as it leads to different distributions for the two walls due to the asymmetric ion distribution in the lamina.

Figure 3 shows three-dimensional plots of $g_{OO}(r\cos\vartheta, r\sin\vartheta)$ with r_{OO} and ϑ as in Eq. (1) where the wall is positioned along the abscissa. Figure 3(a) is calculated from the present simulation for oxygen atoms being close to the walls ($8.0\text{ Å} \leqslant |z_1|$), whereas Fig. 3(b) is for oxygen atoms located in the interior of the lamina. Figures 3(c) and 3(d) correspond to Figs. 3(a) and 3(b) for a simulation of pure ST2 water between two Lennard-Jones walls,[9] respectively. As $r\cos\vartheta$ is the projection of the oxygen–oxygen vector along the inward directed wall normal and $r\sin\vartheta$ is its projection along the wall the drawings illustrate the anisotropy of the oxygen distribution around a central O atom. Curves (b) and (d) have approximately equal heights of the first maximum for all directions but the result for pure water shows a slightly more pronounced second shell structure. A similar difference is found in the isotropic case. Contrarily, curves (a) and (c) show an enormous increase of the first maximum in directions parallel to the wall. Although, due to their one-dimensonal potential, the walls have no direct ordering effect there is increased order in directions parallel to the wall indicating an ice Ih like structure with the c axis parallel to the wall normal (see also Ref. 10). However, the effect on the solution is significantly smaller than on pure water due to the local ionic distribution.

IV. DYNAMICAL RESULTS

A. Translational motion

To investigate the changes in the translational motion of water molecules near the LJ walls velocity autocorrelation functions have been calculated for three layers separately (A: $|z| < 4$ Å; B: $4\text{ Å} \leqslant |z| \leqslant 8.0$ Å; C: $|z| > 8.0$ Å). As the differences between layers A and B are small and resemble mainly the slightly different ion distributions only the functions for the interior of the lamina (average over layers A and B) and the wall layer (C) are given. Thus the subdivisions are the same as in the preceding section.

Because of the anisotropy of the system in the z direction the velocity autocorrelation functions are calculated separately for the component of motion parallel and perpendicular to the walls according to

$$c_{v_i}^{(S)}(\tau) = \langle v_i(0)v_i(\tau)\rangle_{t,N(S)} / \langle v_i(0)^2\rangle_{t,N(S)}, \quad (2)$$

with v_i the velocity component parallel ($i = x, y$) or perpendicular ($i = z$) to the walls. S represents either the wall layer ($S = W$) or the interior of the lamina ($S = I$) and the brackets together with the subscript indicate averages over

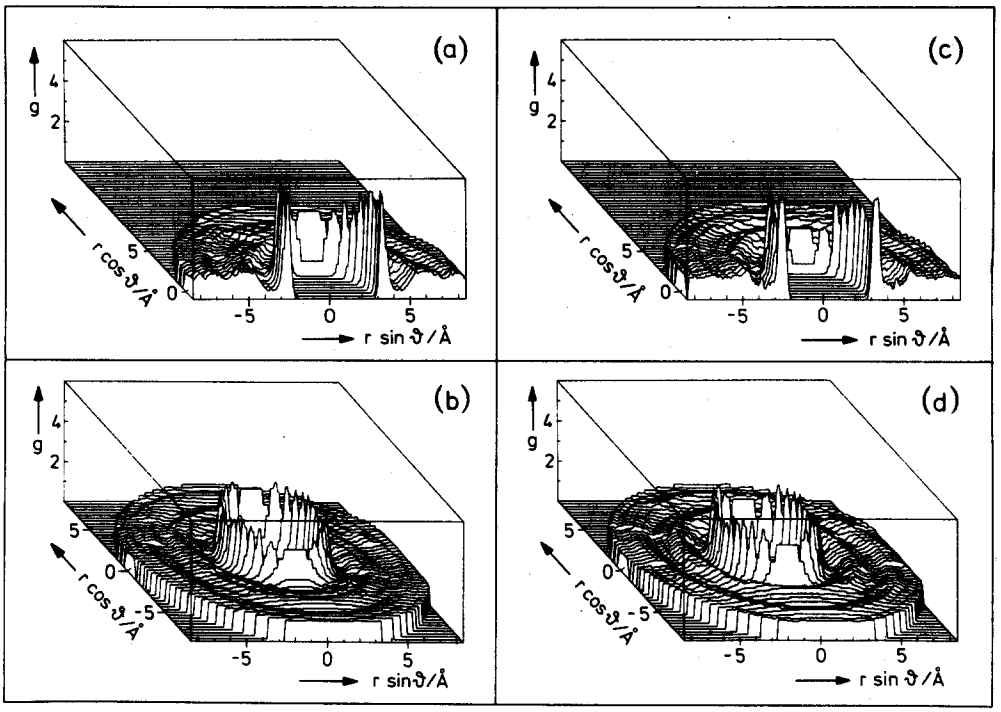

FIG. 3. Anisotropic oxygen–oxygen pair correlation functions g_{OO} ($r\cos\vartheta$, $r\sin\vartheta$) for molecules in the wall layer (a) and in the interior (b) of a 2.2 m aqueous LiI solution between Lennard-Jones walls and the corresponding functions for pure water between Lennard-Jones walls.

starting time (t) and particles [$N(S)$]. Figure 4 shows $c_{v_{xy}}^{(I)}$, $c_{v_{xy}}^{(W)}$, $c_{v_z}^{(I)}$, and $c_{v_z}^{(W)}$ together with their spectral densities calculated by Fourier transformation in the insertions.

A comparison of the autocorrelation functions shows on the one hand pronounced differences between molecules near the interface (W) and those in the interior of the lamina (I) and on the other hand differences for the interphase molecules (W) between vertical and transversal movement relative to the walls ($i = xy$ and z, respectively). Due to the short-ranging water–wall interactions $c_{v_{xy}}^{(I)}$ and $c_{v_z}^{(I)}$ do not differ significantly. They are similar to the ones for the isotropic solution.[15]

The autocorrelation function for water motion parallel to the walls ($c_{v_{xy}}^{(S)}$) shows similar maxima and minima in the wall layer and in the interior which, however, do not lead to a change of sign of the velocity at about 0.07 ps for molecules near the wall. This is partly a consequence of the lower density in the interphasial region and partly due to the fact that the walls do not exhibit any "shear" forces on the molecules which could hinder the translational motion to a similar extent as additional water molecules would do.

Of course, the effect of the walls on the z motion is stronger so that the form of the velocity autorcorrelation function is changed. Obviously the disappearance of the second maximum in the velocity autocorrelation functions which occurs in $c_{v_{xy}}^{(I)}$, $c_{v_{xy}}^{(W)}$, and $c_{v_z}^{(I)}$ after about 0.15 ps is due to the weaker interactions with the walls instead of the comparatively strong water–water interactions. These results are in accordance with those of Sonnenschein and Heinzinger.[9]

The spectral densities of the translational motions which are given in the insertions of Fig. 4 differ for molecules in the interphasial region drastically from those in the interior of the lamina or the isotropic solution.[14] The peak at ≈ 50–$60\ \mathrm{cm}^{-1}$ which is usually assigned to the intermolecular O–O–O bending motion[22] is strongly increased while the shoulder at $\approx 200\ \mathrm{cm}^{-1}$ is weakened both for the motion parallel and perpendicular to the wall. This indicates that the type of motion changes from the normal density region to the low density region becoming more bend-like. The reason

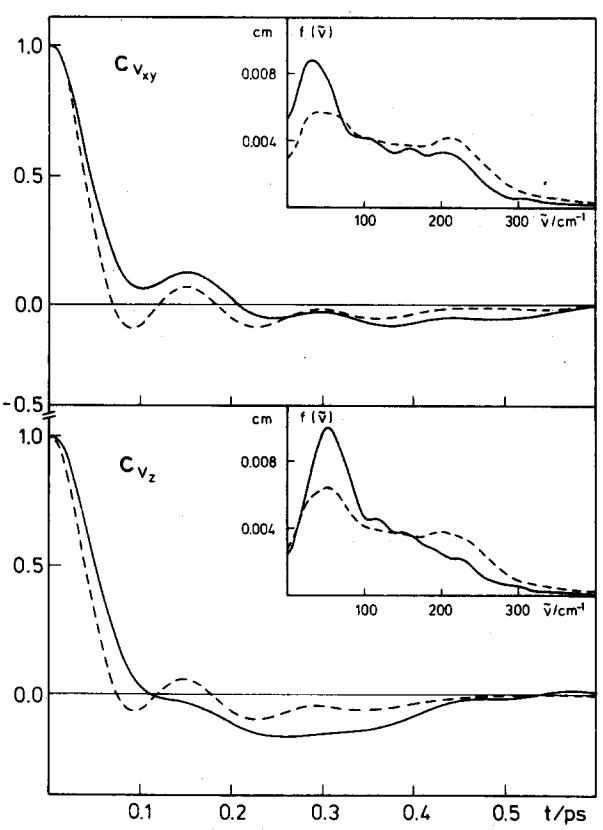

FIG. 4. Oxygen velocity autocorrelation functions $c_{v_i}^{(S)}$ and spectral densities of translational motion (insertions) for motion parallel to the wall ($i = xy$) and perpendicular to the wall ($i = z$) for water molecules close to the wall ($S = W$; full lines) and in the interior of the lamina ($S = I$; dashed lines).

TABLE II. Self-diffusion coefficients for water of the 2.2 m LiI solution and pure water, respectively, between Lennard-Jones type walls at 283 K in units of 10^{-5} cm^2 s^{-1}. $D_i^{(S)}$ are the self-diffusion coefficients for motion parallel ($i = xy$) and perpendicular ($i = z$) to the wall for molecules in the interior ($S = I$) and near the wall ($S = W$). D^{tot} is the average value for the whole lamina and D^{iso} the value of the bulk solution and bulk water, respectively.

	$D_{xy}^{(W)}$	$D_z^{(W)}$	$D_{xy}^{(I)}$	$D_z^{(I)}$	D^{tot}	D^{iso}
LiI[a]	4.1	3.7[d]	2.4	2.4	2.4	2.0[b]
H_2O[c]	4.7	4.8[d]	2.8	3.5	3.1	2.8[b]

[a] This work.
[b] Data from Ref. 14 extrapolated to 283 K.
[c] Data from Ref. 9 extrapolated to 283 K.
[d] The Kubo equation cannot be applied. The self-diffusion coefficients were calculated using the method given in Ref. 9.

for that is that the average structure near the walls is more tetrahedral, thus favoring the bend type motion in which one molecule tries to move through the gap between two others. This conclusion is supported by a reverse effect found in an MD simulation of high density water that used a modified central force potential to describe the water–water interactions[23] where the O–O–O bending mode was reduced in the high density simulation relative to the normal density water.

The self-diffusion coefficients have been calculated from the Green–Kubo relation

$$D_i^{(S)} = \lim_{t\to\infty} \int_0^t c_{v_i}^{(S)}(\tau)\,d\tau. \tag{3}$$

The resulting $D_i^{(S)}$ are compared in Table II with those for pure ST2 water between Lennard-Jones walls[9] and for the isotropic LiI solution.[15]

The following conclusions can be drawn from the results: (i) The motion along the walls is significantly faster in both simulations with LJ walls as compared to the motion in the inner part of the lamina or in the isotropic system. The observed increase of the diffusion coefficient is in agreement with the reduced solvation energy of a water molecule in the wall layer which is due to the decrease in the number of hydrogen bonds. (ii) The total self-diffusion coefficients D^{tot} are greater for both anisotropic simulations thus indicating—contrary to the absence of a wall effect on the structural behavior inside the lamina—an influence of the walls on the dynamics of the whole lamina. (iii) The effect of the walls on the self-diffusion coefficient of the LiI solution is similar to that on pure water.

B. Rotational motion

Figure 5 shows the angular velocity autocorrelation functions

$$c_{\omega_i}^{(S)}(\tau) = \langle \omega_i(0)\omega_i(\tau)\rangle_{t,N(S)} / \langle \omega_i(0)^2\rangle_{t,N(S)} \tag{4}$$

for the interphasial (W) and the inner region (I) separately for the rotations about the three body-fixed axes (defined in the insertion).

All rotations about the principal axes of the water molecules in the interphasial region show a tendency to preserve their motion for longer times than in the inner part of the solution as can be seen from the shift of the first zeros of the

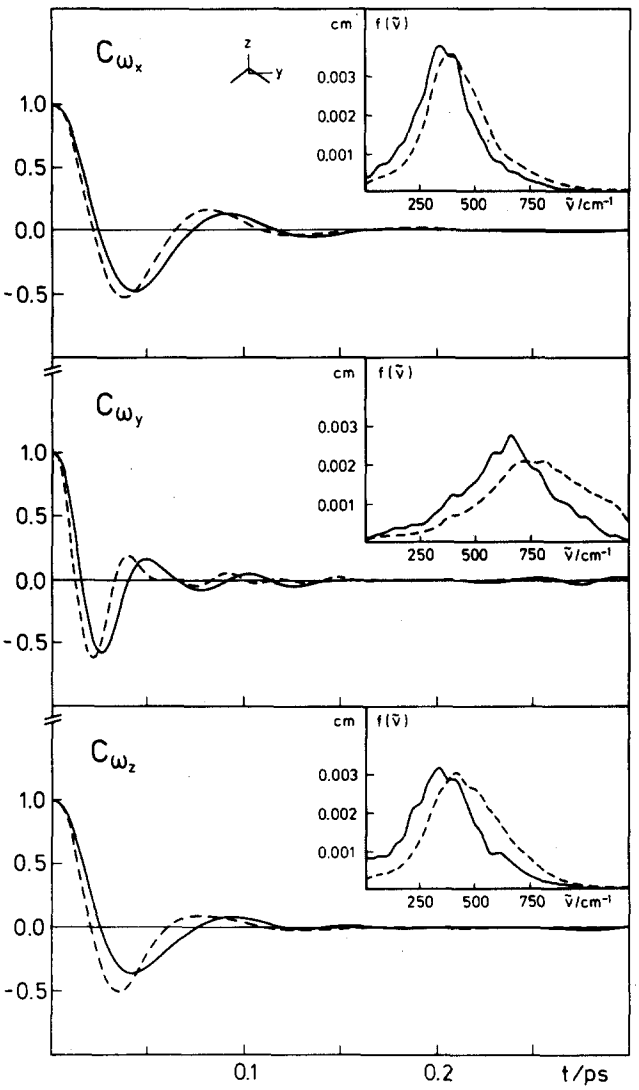

FIG. 5. Angular velocity autocorrelation functions $c_{\omega_i}^{(S)}$ and spectral densities of rotational motion of water molecules for rotations about the three principal molecular axes ($i = x, y, z$) for water molecules close to the walls (full lines) and in the interior of the lamina (dashed lines).

autocorrelation functions to longer times. Accordingly, the spectral densities of the rotational motion shown in the insertions of Fig. 5 are shifted by about 60–100 cm^{-1} to lower wave numbers (see Table III) which results from the reduced number of hydrogen bonds in the interphase.

The rotational diffusion coefficients

$$^rD_i^{(S)} = \lim_{t\to\infty} \int_0^t c_{\omega_i}^{(S)}(\tau)\,d\tau \tag{5}$$

are given in Table III. They are slightly increased for the rotation about the x and y axis but drastically enhanced (by more than a factor of 2) for the rotation about the dipole axis. The comparatively strong effect on the diffusion constant $^rD_z^{(W)}$ and the relatively larger shift for the libration around the z axis is a consequence of the fact that the water dipole vector (z axis) in the wall layer is preferentially oriented parallel to the wall whereas the orientational distribution of the other two axes relative to the wall is found to be

TABLE III. Rotational diffusion coefficients ${}^{r}D_i^{(S)}$ of water for rotations about the three principal axes of intertia ($i = x, y, z$) for molecules in the interior of the lamina ($S = I$) and near the walls ($S = W$) and frequency shifts $\Delta\tilde{\nu}_i$ of the maximum of the spectral density of the librations.

i	x	y	z
${}^{r}D_i^{(W)}/10^{-12}\,s^{-1}$	0.34	0.62	0.99
${}^{r}D_i^{(I)}/10^{-12}\,s^{-1}$	0.27	0.56	0.45
$\Delta\tilde{\nu}_i/cm^{-1}$	60	100	75

uniform. Hence, the rotation about the dipole axis is most influenced by the absence of approximately one hydrogen bond.

V. CONCLUSIONS

The results of an MD simulation of a 2.2 m aqueous LiI solution between two unpolar walls have shown an increase in the hydration shell structure of the iodide ion whereas the strongly hydrated Li cation is not influenced by the weak interactions with the walls. The water structure near the wall tends to be more ice-like than in the interior of the lamina. Simultaneously the type of motion of water molecules in the interphasial region has changed and the self-diffusion coefficients for translational and rotational motions are increased.

[1]P. V. Giaquinta and M. Parinello, J. Chem. Phys. **78**, 1946 (1983).
[2]P. V. Giaquinta and M. Parinello, J. Chem. Phys. **81**, 4074 (1984).
[3]A. Hamelin, T. Titanov, E. Sevastyanov, and A. Popov, J. Electroanal. Chem. Interfacial Electrochem. **145**, 225 (1983).
[4]D. L. Doering and T. E. Madey, Surf. Sci. **123**, 305 (1982).
[5]B. Jönsson, Chem. Phys. Lett. **82**, 520 (1981).
[6]N. I. Christou, J.-S. Whitehouse, D. Nicholson, and N.-G. Parsonage, Faraday Symp. Chem. Soc. **16**, 139 (1981).
[7]M. Marchesi, Chem. Phys. Lett. **97**, 224 (1983).
[8]G. Barabino, C. Gavotti, and M. Marchesi, Chem. Phys. Lett. **104**, 478 (1984).
[9]R. Sonnenschein and K. Heinzinger, Chem. Phys. Lett. **102**, 550 (1983).
[10]C. Y. Lee, J. A. McCammon, and P. J. Rossky, J. Chem. Phys. **80**, 4448 (1984).
[11]R. M. Townsend, J. Gryko, and S. A. Rice, J. Chem. Phys. **82**, 4391 (1985).
[12]N. Anastasiou, D. Fincham, and K. Singer, J. Chem. Soc. Faraday Trans. 2 **79**, 1639 (1983).
[13]Gy. I. Szász, K. Heinzinger, and W. O. Riede, Z. Naturforsch. Teil A **36**, 1067 (1981).
[14]Gy. I. Szász and K. Heinzinger, J. Chem. Phys. **79**, 3467 (1983).
[15]Gy. I. Szász, K. Heinzinger, and W. O. Riede, Ber. Bunsenges. Phys. Chem. **85**, 1056 (1981).
[16]R. Sonnenschein, Ph. D. thesis, Mainz, F. R. Germany, 1984.
[17]F. H. Stillinger and A. Rahman, J. Chem. Phys. **60**, 1545 (1974).
[18]D. M. Heyes, Daresbury Laboratory Inf. Q. Comput. Sim. Condensed Phases **9**, 20 (1983).
[19]H. M. Evjen, Phys. Rev. **39**, 675 (1932).
[20]S. Toxvaerd, J. Chem. Phys. **74**, 1998 (1981).
[21]F. Vesely, *Computerexperimente an Flüssigkeitsmodellen* (Physik Verlag, Weinheim, 1978).
[22]M. G. Sceats and S. A. Rice, J. Chem. Phys. **72**, 3236 (1980).
[23]G. Jancsó, P. Bopp, and K. Heinzinger, Chem. Phys. **85**, 377 (1984).